Supplement of Hydrol. Earth Syst. Sci., 30, 3185–3201, 2026
https://doi.org/10.5194/hess-30-3185-2026-supplement

Hydrology and Earth System Sciences
Open Access
EGU

Supplement of

Shifting water scarcities: irrigation alleviates agricultural green water deficits while increasing blue water scarcity

Heindriken Dahlmann et al.

Correspondence to: Heindriken Dahlmann (heindriken.dahlmann@hu-berlin.de)

Model setup

CFT categories

LPJmL covers 12 crop functional types (CFTs), including: temperate cereals, rice, maize, tropical cereals, pulses, temperate roots, tropical roots, sunflower, soybean, groundnut, rapeseed, sugar cane, in addition to an "others" category (see Schaphoff et al. (2018)). We adopt 100% of the cropland area from the HYDE database, which corresponds to 100% of the FAO cropland. However, a significant share of this area may be classified as the category "others", which aggregates all crops not parameterised specifically as CFTs. Many FAOSTAT primary crops fall under this "others" category, e.g. all FAO primary crops of the category "Seeds & Oils" except sunflower and rapeseed, and also many vegetables. "Others" include also some perennial crops, e.g. coffee, cocoa and tea. The 12 parameterised CFTs cover ≈ 60% of the global agricultural area while "others" cover ≈ 40%.

Irrigation

To determine which irrigation method to apply to each CFT, decision rules have been developed by Jägermeyr et al., 2015 (based on Brouwer et al., 1988; Sauer et al., 2010; Fischer, 2012). These rules specify the suitability of surface, sprinkler, and drip systems for each CFT (summarized in Jägermeyr et al., 2015, Table 2). For all CFTs that may be suitable for more than one irrigation method, a structured allocation algorithm was applied: First, for each country, all grid cells with drip-suitable CFTs were identified, and CFT fractions were randomly sampled until the national target area for drip irrigation was met. This procedure was repeated 1000 times, and the iteration best matching the national target was selected. Second, sprinkler irrigation was assigned following the same logic, and the remaining irrigated area was allocated to surface systems (see Jägermeyr et al., 2015 (Supplementary Material)). In this way, the method selection is not based solely on CFT suitability but also constrained by observed national irrigation system shares. As a result, each CFT in each grid cell is allocated to one of the three irrigation systems. The parameterisation of irrigation efficiency depends on the irrigation systems as well as soil conditions. For pressurized systems (sprinkler and drip irrigation), the conveyance efficiency is set to 0.95 while for surface irrigation conveyance efficiency is connected to different soil saturated hydraulic conductivities (see Jägermeyr et al., 2015 (Table 1)). The irrigation efficiency values are based on the area-weighted shares of irrigation systems at the grid-cell level.

Model runs

Figure S1 provides a schematic representation of the LPJmL model runs. The 3,500-year spin-up period has been applied for the natural vegetation in order to bring the plant functional type (PFT) distributions as well as the carbon and nitrogen pools into a dynamic pre-industrial equilibrium. This spin-up is generally needed so that pool sizes and simulated dynamics are not affected by model drift or inconsistencies between an initialization of pools and internally computed rates. The subsequent land-use spin-up (1500-2014), allows the model to incorporate historical land-use changes. From 1901 onwards, we have a

transient climate input, which is needed for including the effect of historical land use and climate on agricultural soil properties, amongst others. After this, the analysis period (2015-2019) starts.

We ran a limited irrigation run (ILIM), distinguishing between rainfed and irrigated agriculture. Irrigation in this run depends on water availability in rivers, reservoirs and upstream neighbouring cells from which irrigation water can also be withdrawn. For the analyses of this paper, we ran a second irrigation scenario which neglects irrigation and considers all agriculture to be rainfed (INO). For better comparability of irrigated CFTs in INO and ILIM, the growing seasons of the concerned CFTs in INO are adjusted so that they retain their actual growing season length (as in ILIM) and do not adapt to the rainfed growing season. Furthermore, a groundwater buffer represents subsurface water storage and sustains baseflow during dry periods by releasing water at a fixed rate of 0.01 d^{-1} relative to its volume (based on Döll et al., 2003), simulating a simplified renewable groundwater discharge. While shallow groundwater is implicitly included in the baseflow scheme, the groundwater reservoir operates independently from soil moisture processes; thus, capillary rise and direct renewable groundwater inflows are not explicitly represented. Instead, these inflows are implicitly captured through drainage from the lowest soil layer contributing to river discharge.

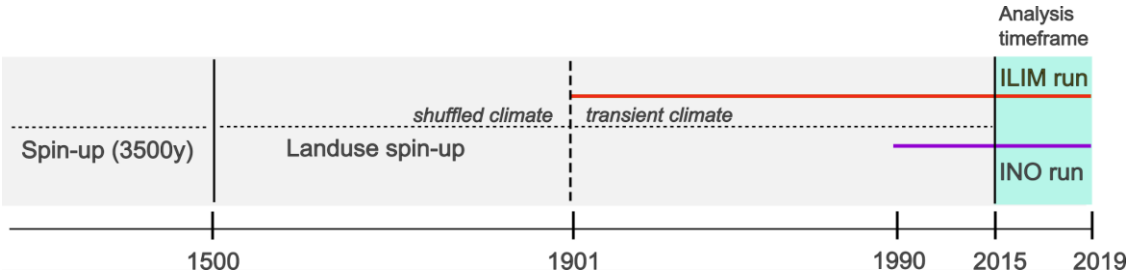

Figure S1: Schematic representation of the LPJmL model runs.

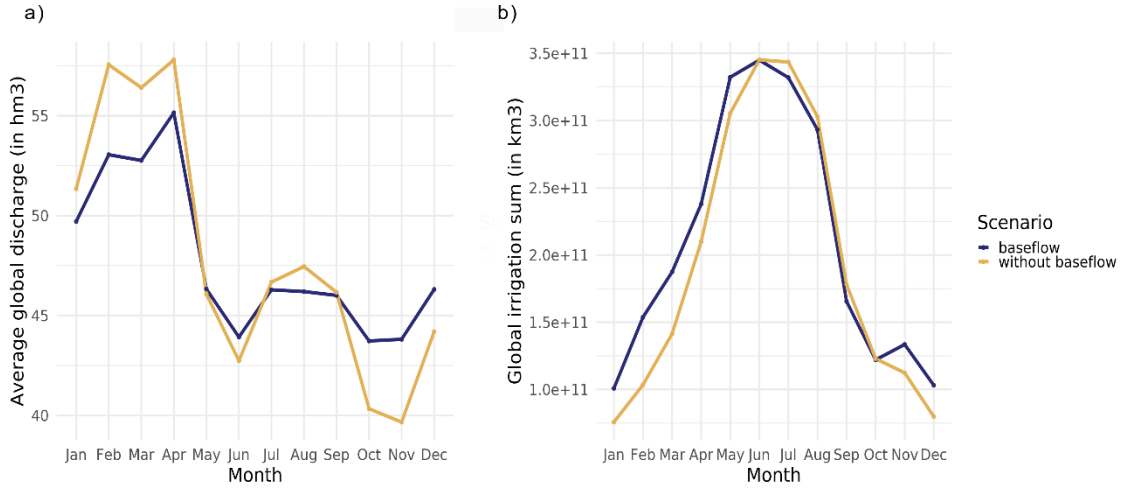

Figure S2: Comparison of a) the average global discharge and b) the global irrigation sum with and without the implemented baseflow.

rainfed temperate cereals
Summer (March - August)

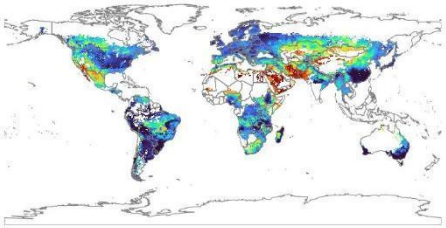

rainfed temperate cereals
Winter (September - February)

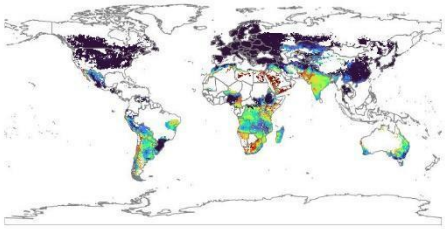

rainfed rice
Summer (March - August)

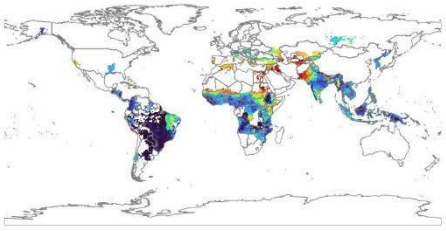

rainfed rice
Winter (September - February)

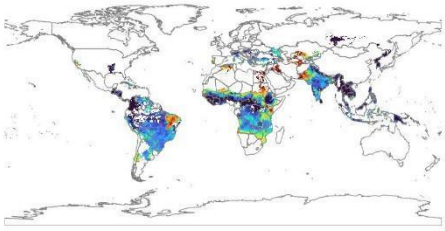

rainfed maize
Summer (March - August)

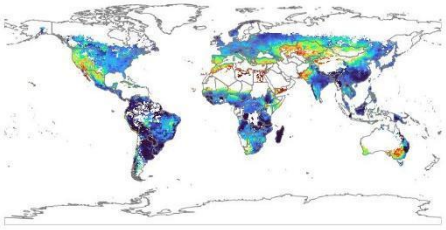

rainfed maize
Winter (September - February)

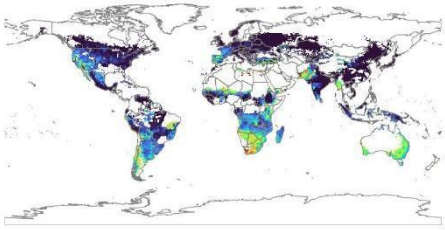

rainfed tropical cereals
Summer (March - August)

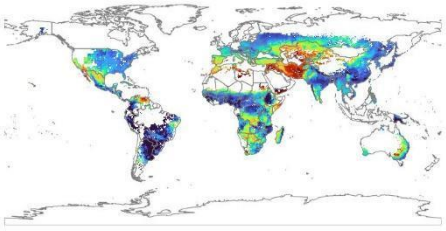

rainfed tropical cereals
Winter (September - February)

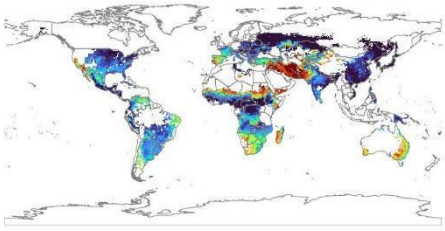

rainfed pulses
Summer (March - August)

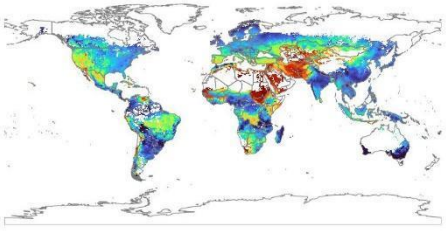

rainfed pulses
Winter (September - February)

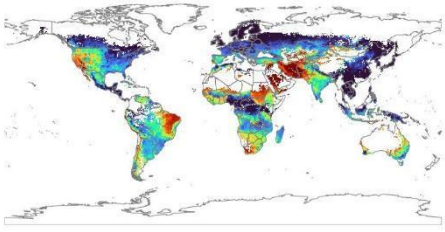

rainfed temperate roots
Summer (March - August)

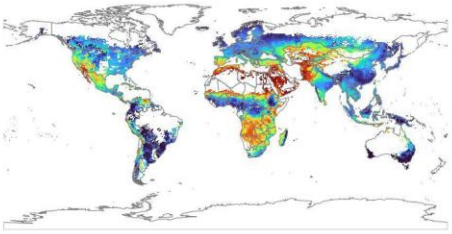

rainfed temperate roots
Winter (September - February)

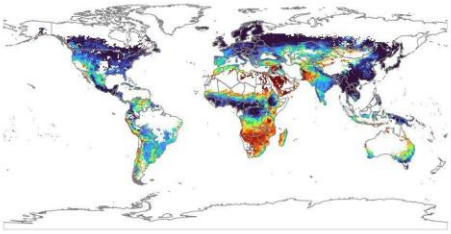

rainfed tropical roots
Summer (March - August)

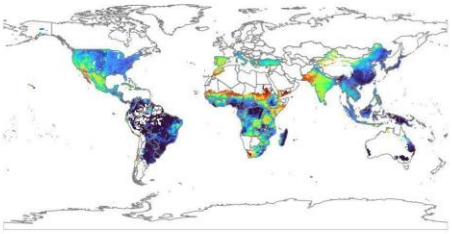

rainfed tropical roots
Winter (September - February)

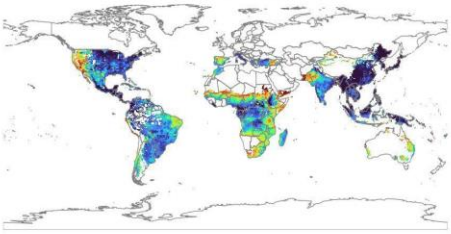

rainfed oil crops sunflower
Summer (March - August)

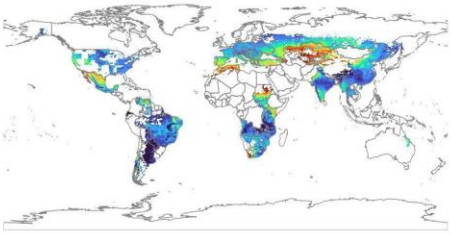

rainfed oil crops sunflower
Winter (September - February)

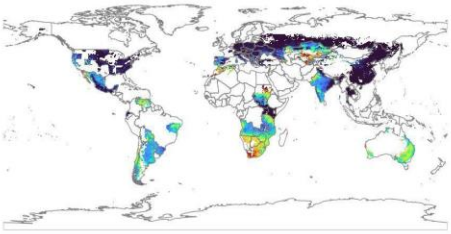

rainfed oil crops soybean
Summer (March - August)

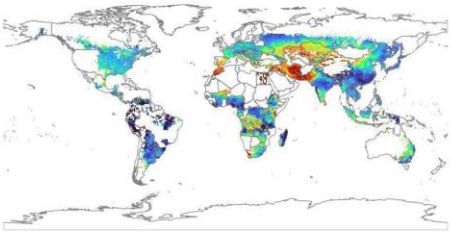

rainfed oil crops soybean
Winter (September - February)

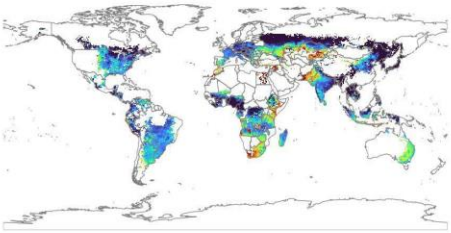

rainfed oil crops groundnut
Summer (March - August)

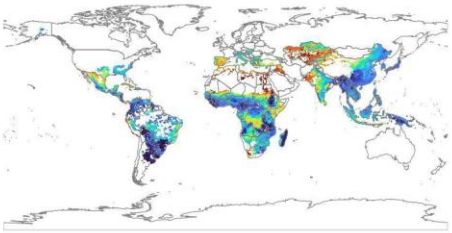

rainfed oil crops groundnut
Winter (September - February)

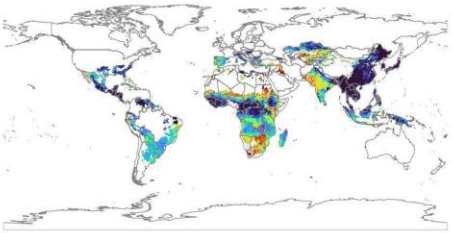

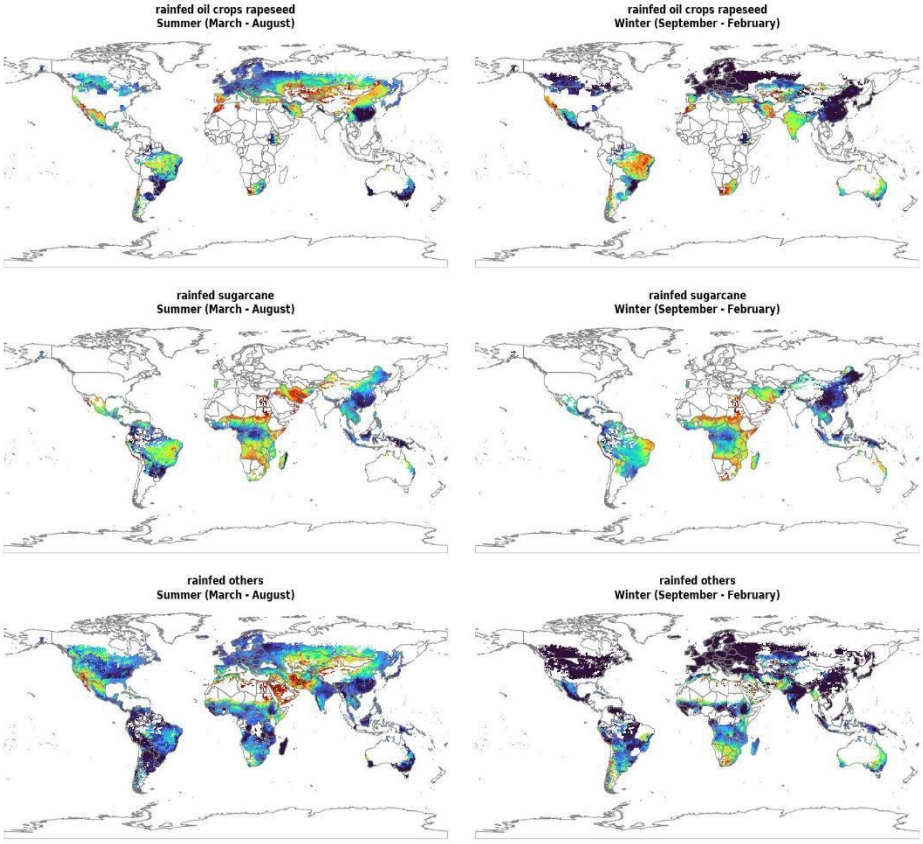

Figure S3: CFT-specific GWS of the rainfed CFTs in the ILIM scenario (averaged over the 2015-2019 for the summer and winter months).

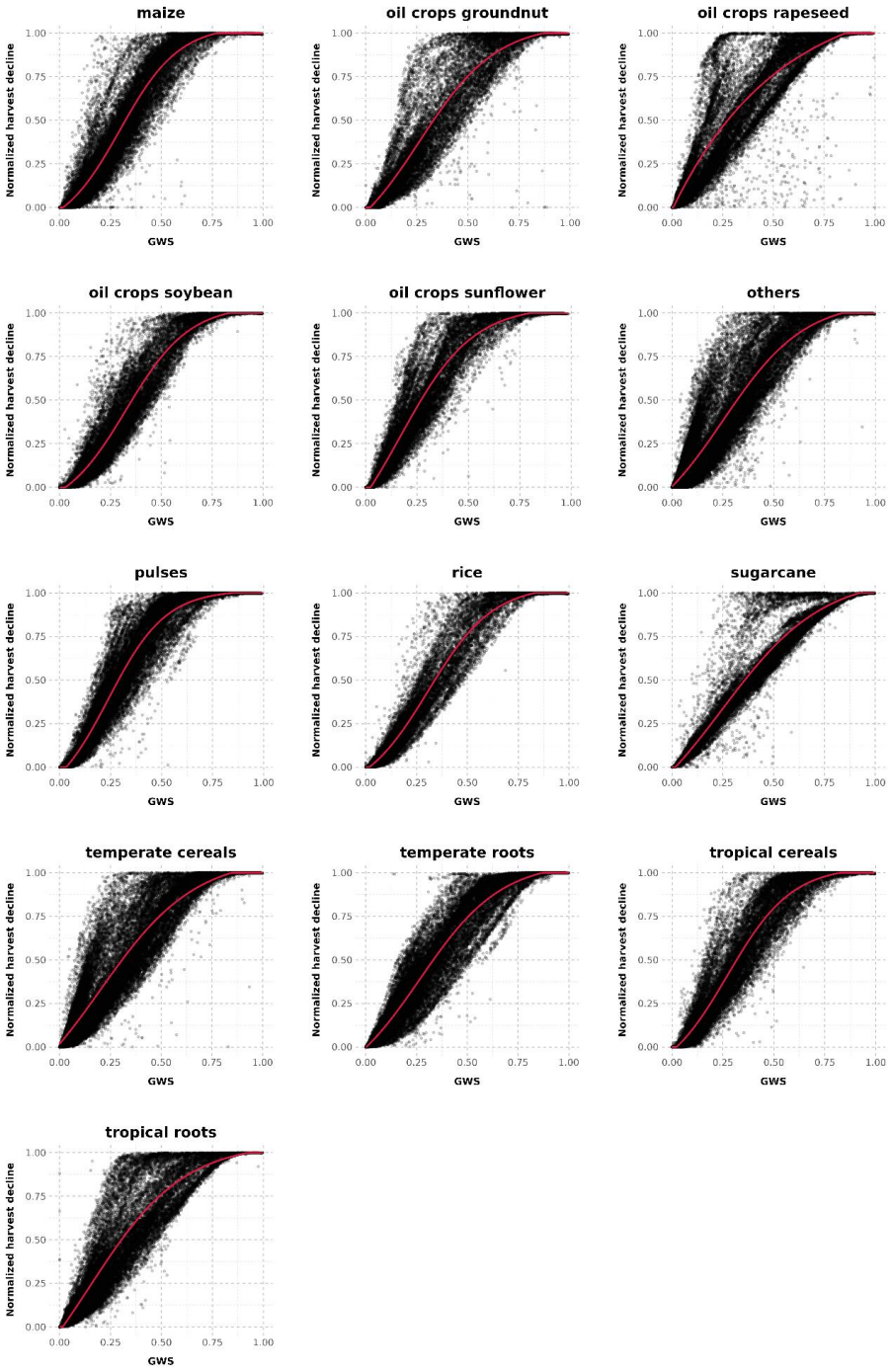

Figure S4: CFT-specific relationships between GWS and yield decline: Normalized yield decline from $IALL_{threshold}$ (optimal yield scenario without water or nitrogen limitation) to $INO_{threshold}$ (water-limited scenario) attributable to GWS ($INO_{threshold}$).

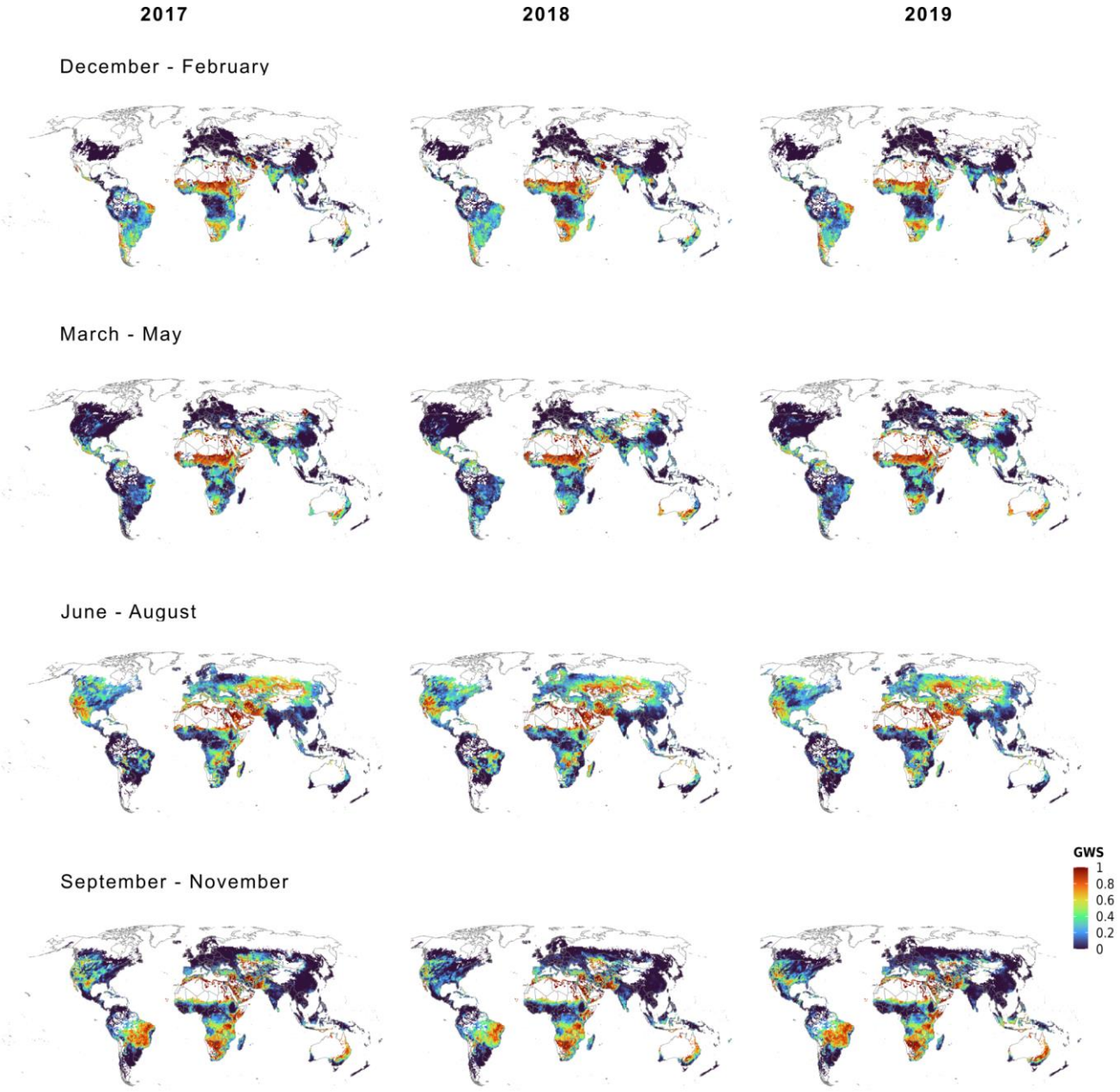

Figure S5: Comparison of GWS in different years. GWS on a seasonal scale, averaged over all CFTs in ILIM for the years 2017, 2018 and 2019.

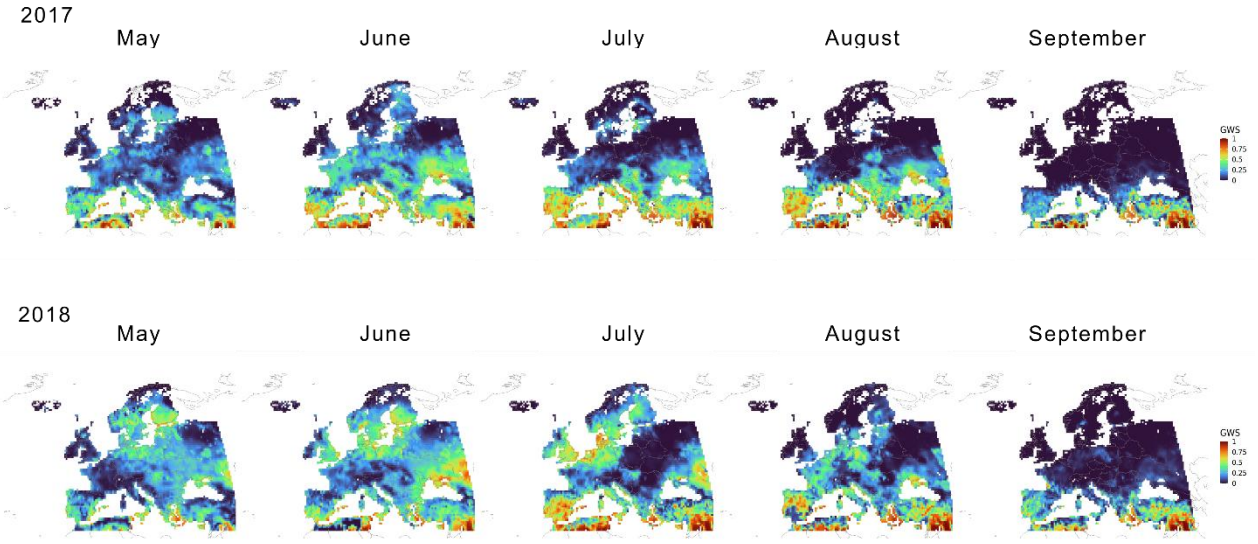

Figure S6: Comparison of GWS in the summer months in Europe in 2017 and 2018.

65

Table S1: GWS thresholds of all CFTs.

	Low GWS	Moderate GWS	High GWS	Severe GWS	Extreme GWS
Maize	< 0.17	0.17 - 0.27	0.27 - 0.37	0.37 - 0.49	> 0.49
Oil crops groundnut	< 0.16	0.16 - 0.27	0.27 - 0.39	0.37 - 0.54	> 0.54
Oil crops rapeseed	< 0.10	0.10 - 0.21	0.21 - 0.35	0.35 - 0.54	> 0.54
Oil crops soybean	< 0.19	0.19 - 0.30	0.30 - 0.41	0.41 - 0.54	> 0.54
Oil crops sunflower	< 0.12	0.12 - 0.22	0.22 - 0.32	0.32 - 0.46	> 0.46
Others	< 0.14	0.14 - 0.26	0.26 - 0.38	0.38 - 0.53	> 0.53
Pulses	< 0.15	0.15 - 0.24	0.24 - 0.34	0.34 - 0.46	> 0.46
Rice	< 0.17	0.17 - 0.29	0.29 - 0.39	0.39 - 0.53	> 0.53
Sugarcane	< 0.16	0.16 - 0.29	0.29 - 0.43	0.43 - 0.60	> 0.60
Temperate cereals	< 0.12	0.12 - 0.24	0.24 - 0.37	0.37 - 0.54	> 0.54
Temperate roots	< 0.15	0.15 - 0.27	0.27 – 0.40	0.40 - 0.55	> 0.55
Tropical cereals	< 0.16	0.16 - 0.27	0.27 - 0.37	0.37 – 0.50	> 0.50
Tropical roots	< 0.13	0.13 - 0.24	0.24 - 0.37	0.37 - 0.54	> 0.54

Table S2: CFT-specific green water stressed areas in the ILIM run (average 2015-2019)

	Low GWS	Moderate GWS	High GWS	Severe GWS	Extreme GWS
Maize	112 Mha	41 Mha	12 Mha	6 Mha	2 Mha
Oil crops groundnut	8 Mha	5 Mha	4 Mha	4 Mha	3 Mha
Oil crops rapeseed	14 Mha	4 Mha	7 Mha	3 Mha	1 Mha
Oil crops soybean	52 Mha	36 Mha	8 Mha	2 Mha	1 Mha
Oil crops sunflower	3 Mha	7 Mha	9 Mha	4 Mha	1 Mha
Others	387 Mha	121 Mha	76 Mha	48 Mha	26 Mha
Pulses	20 Mha	17 Mha	18 Mha	11 Mha	14 Mha
Rice	90 Mha	10 Mha	5 Mha	3 Mha	2 Mha
Sugarcane	10 Mha	3 Mha	5 Mha	2 Mha	0 Mha
Temperate cereals	153 Mha	43 Mha	27 Mha	16 Mha	5 Mha
Temperate roots	13 Mha	5 Mha	1 Mha	1 Mha	1 Mha
Tropical cereals	22 Mha	13 Mha	9 Mha	9 Mha	16 Mha
Tropical roots	9 Mha	10 Mha	7 Mha	4 Mha	1 Mha

Table S3: Agricultural area affected by GWS in cells with irrigation (average 2015-2019).

	INO	ILIM
Low GWS	316 Mha (46%)	456 Mha (66%)
Moderate GWS	158 Mha (23%)	113 Mha (16%)
High GWS	90 Mha (13%)	60 Mha (9%)
Severe GWS	73 Mha (11%)	35 Mha (5%)
Extreme GWS	51 Mha (7%)	24 Mha (4%)

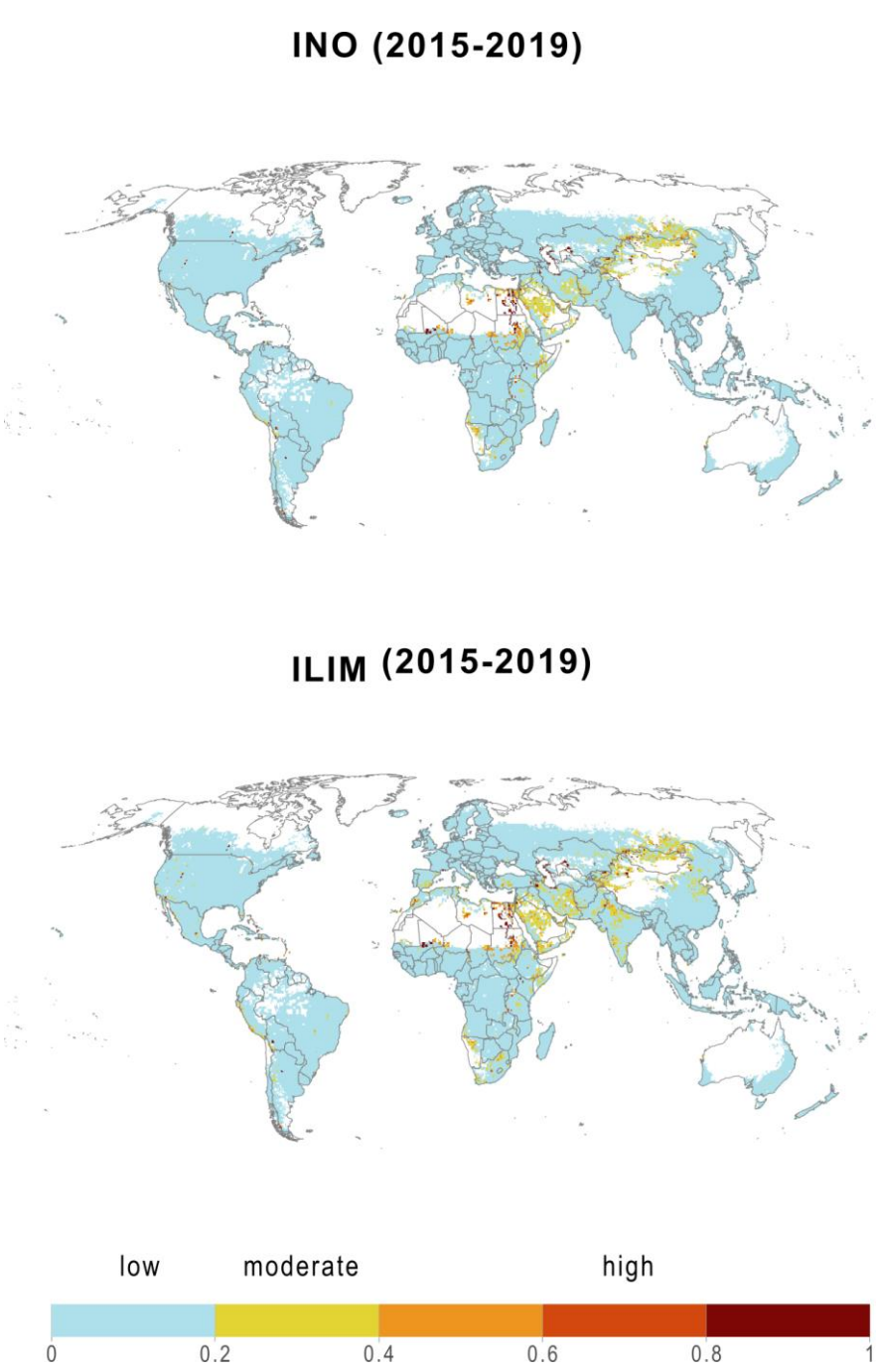

Figure S7: Blue water stress for INO and ILIM (average over time period 2015-2019).

Table S4: Agricultural area affected by BWS in cells with irrigation (average 2015-2019).

	INO	**ILIM**
Low BWS	676 Mha (98%)	580 Mha (84%)
Moderate BWS	8 Mha (1%)	89 Mha (13%)
High BWS	5 Mha (1%)	20 Mha (3%)

Data comparison and validation

For a comparison with the results of He and Rosa (2023), we adjusted our baseline to theirs (1996-2005) and compared the results of both green water stresses. The results show that with our GWS indicator, more severe GWS occurs in Africa and South America, but less in the USA and Europa. The limited GWS observed in the USA and Europe in our study is primarily due to the low atmospheric demand of crops grown during autumn and winter. In these regions, only a few CFTs are cultivated, mainly temperate cereals, tropical cereals, temperate roots, and oil crops such as sunflower, soybean, and rapeseed. For instance, temperate cereals experience GWS from May to August but not for the rest of the year if they are growing (see C9). Similarly, winter rapeseed, predominantly grown in Europe, does not face GWS between September and March. These seasonal patterns significantly influence the average GWS levels. The high GWS patterns He and Rosa (2023) found in the USA are only visible in the summer months in our analysis.

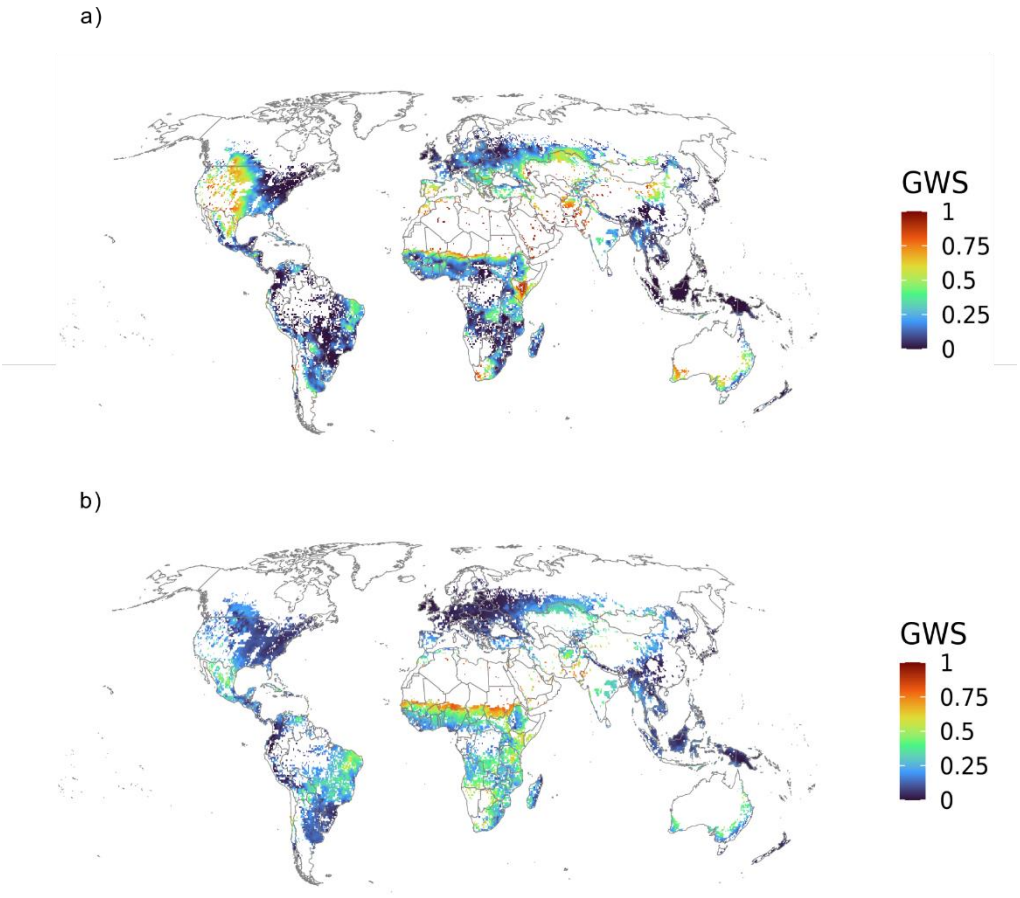

Figure S8: Comparison of GWS in this study to results of He and Rosa (2023): a) average GWS for time period 1996-2005 in He and Rosa (2023), b) average GWS of this study computed for time period 1996-2005 and cropped to spatial extent of He and Rosa (2023).

We further compared our results with the often used actual to potential evapotranspiration (AET/PET) ratio. The plant-specific GWS indicator developed in this study differs from the AET/PET ratio, as the latter reflects broader energy levels. Moreover, the AET/PET ratio accounts for total vegetation across all months within a grid cell, rather than focusing on crop-specific growing seasons. Nonetheless, regions with a high GWS indicator in our analysis tend to coincide with areas where the AET/PET ratio indicates drier conditions.

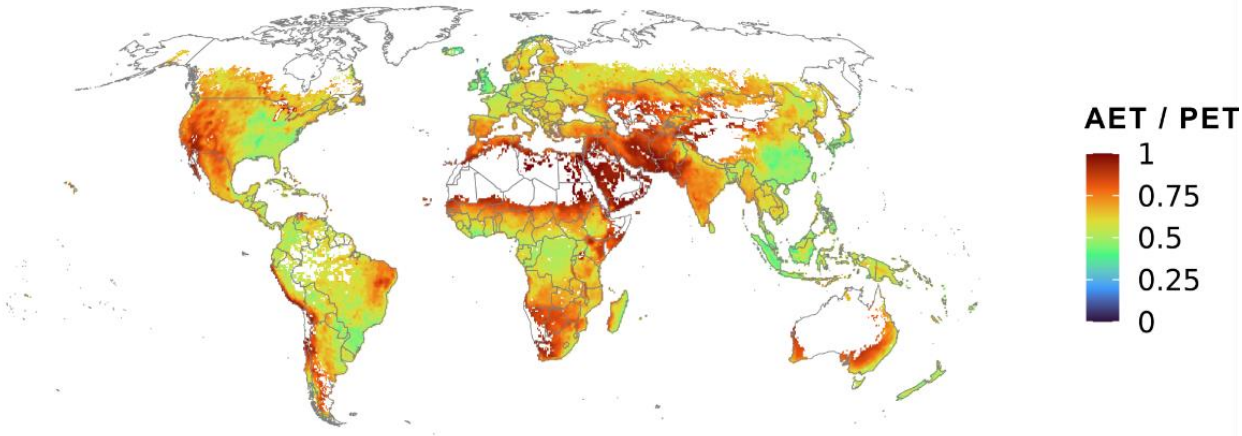

Figure S9: Actual evapotranspiration divided by potential evapotranspiration index (AET/PET) as average for the time period 2015-2019.

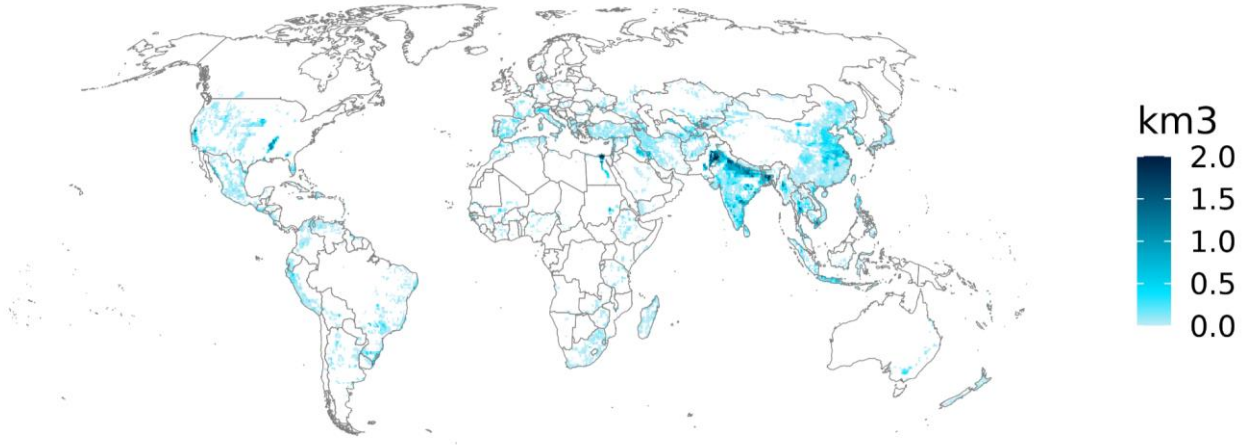

Figure S10: Blue water consumption of this study (annual average 2015-2019)

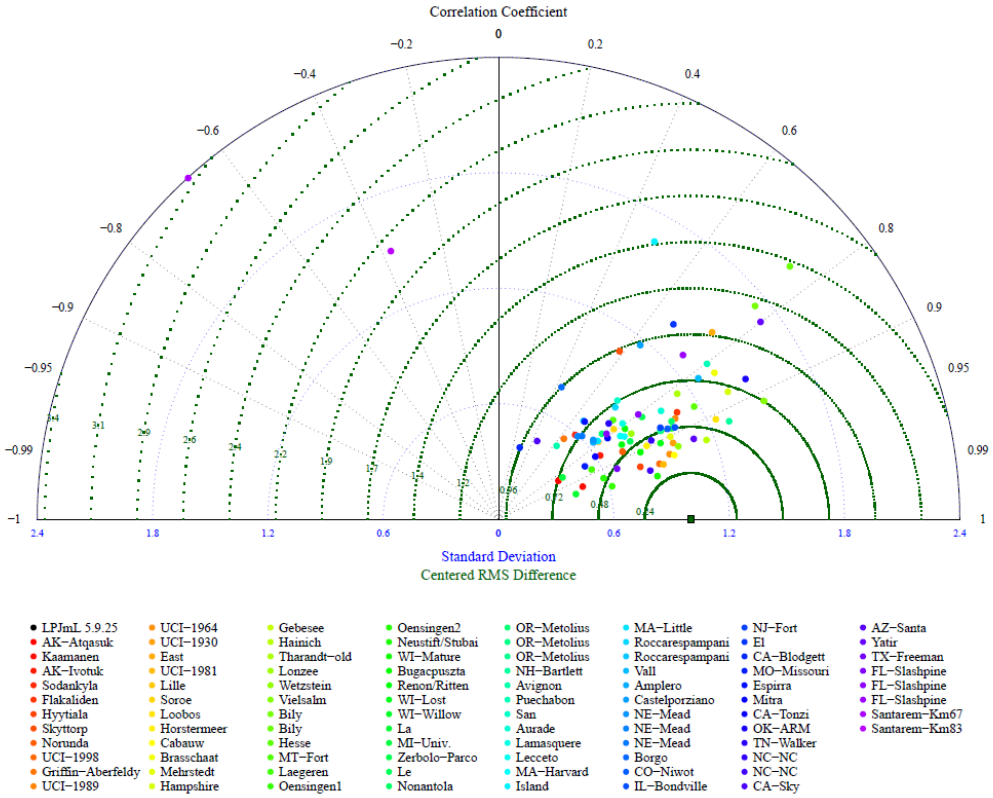

Figure S11: Validation of LPJmL 5.9.25 evaporation rates with evaporation rates measured at eddy flux towers: ORNL DAAC (2011). Available online at FLUXNET (http://fluxnet.fluxdata.org/data/la-thuile-dataset/). Site locations are ordered from north to south.